Research Article | Vol. 29, No. 15 / 19 July 2021 / Optics Express 23167
Optics EXPRESS

Dynamically stable single frequency ring resonator from diode pumped Nd:YAG modules with 55.6 W of output power

ALLAN BERECZKI, AMAURI AGOSTINHO FERREIRA, AND NIKLAUS URSUS WETTER*

Centro de Lasers e Aplicações, IPEN-CNEN/SP, Av. Professor Lineu Prestes, 2242, São Paulo (SP), Brazil
**nuwetter@ipen.br*

Abstract: A Nd:YAG rod single-frequency ring laser based on side-pumped commercial modules is presented. Thermally induced birefringence compensation was applied in a dynamically stable resonator providing 55.6 W of continuous, linearly polarized, TEM_{00} output. The particular case of a symmetric ring resonator containing one or two focusing rods and a pair of curved mirrors was analyzed and a design technique is presented, allowing for easy, continuous shaping of the stability limits by changing only the distances in the resonator.

1. Introduction

Of all solid-state lasers (SSLs), by far the most commonly used laser crystal continues to be the Nd:YAG and, therefore, any improvement that can mitigate the well-known drawbacks in the crystal's characteristics is of major importance [1,2]. Amongst the many positive characteristics of this crystal are its mechanical strength, moderately high absorption and emission cross-sections and the very good thermal conductivity, which is better than for many newer materials, such as vanadates like Nd:$GdVO_4$ and Nd:YVO_4, whereas its major drawback, for many applications, is its absence of natural birefringence [3,4]. Today's solid-state lasers, which are in most cases either diode- pumped (DPSSL) or lamp-pumped (LPSSL), are generally limited in output power, efficiency and beam quality by thermal loading caused by the absorbed pump power. Below the thermally induced stress fracture limit, thermal loading causes, amongst many other detrimental effects, mainly thermally induced lensing and birefringence (TIB). It is this stress-induced birefringence that causes depolarization and bi-focusing in the absence of natural birefringence [5]. In a Nd:YAG crystal with cylindrical geometry, the principal stress-induced birefringent axes are radial and tangential and therefore, depolarization is highest at a 45 degree angle to any polarization axis that is introduced into the resonator [3,4].

Many applications of SSLs require polarized beams of high quality (generally TEM_{00} mode operation) and therefore TIB needs to be compensated for, or the polarization devices will cause very high losses and beam-degradation. Traditionally TIB is mitigated by including a 90° polarization rotation between two identical rods either by placing a half-wave-plate (HWP) between the rods or by using only one rod, a quarter-wave-plate and a highly reflecting mirror [6,7]. Polarization rotation alone is no guarantee for TIB compensation because thermally induced bi-focusing leads to a spatial separation of the polarized beam components and causes the beam path to bend with different beam radii and beam sizes inside the active element [8]. Therefore additional optical elements are generally used to image the rod's principal plane onto itself, in the case of one single rod, or onto each other, in the case of two rods [9,10]. This can be achieved by a single curved mirror in the case of one rod or, relay-imaging optics, consisting generally of two lenses, in the case of two rods [11]. It has been shown that complete birefringence compensation under thermal lensing is possible in standing wave cavities for the case of a quadratic transverse refractive index variation [9]. In real systems, the alignment of

#430327 https://doi.org/10.1364/OE.430327
Journal © 2021 Received 7 May 2021; revised 17 Jun 2021; accepted 28 Jun 2021; published 7 Jul 2021

Optics EXPRESS

the imaging system is complex because only in very special cases complete compensation is achieved by mutual imaging of the rod's principal planes [12].

When considering side-pumped lasers, output power is proportional to the laser mode volume inside the active media and therefore a large stationary TEM_{00} beam waist is desirable. Additionally, for high beam quality and single frequency operation, oscillation of higher order transversal modes must be prevented. In order to reach this goal, the dynamically stable resonator (DSR) technique, developed by Magni et al. [13], uses a large stationary TEM_{00} beam waist, w_{30}, inside the rod whereas the rod diameter itself is the limiting aperture for higher order modes. However, for increasing beam waists TIB causes a separation between the radial and tangential stability intervals of the resonator, to a point where they cease to overlap, impeding simultaneous oscillation of both polarizations. This limits the maximum achievable beam radius, w_{30}, to approximately 1.1 mm inside the Nd:YAG rod, with w_{30} being typically between 50% to 83% of the rod radius [14].

One approach to deal with this problem is the use of joined stability zones, allowing both radial and tangential polarizations to oscillate in separate stability zones each, allowing thereby for a larger beam waist [15–17]. However, standing wave cavities with joined stability zones will always show a discontinuity in the middle of the stability interval. The ring resonator shows much more favorable characteristics, presenting a single, continuous and, especially, twice as wide stability zone, [18].

Ring resonators have many important applications: They are the preferred type for single frequency lasers because of their travelling wave nature that can eliminate spatial hole-burning and, they also demonstrated an order of magnitude higher output powers in single-frequency operation when compared to linear cavity lasers [19]. Other characteristics of ring lasers are low sensitivity to misalignment in the plane of the ring and the fact that additional intra-cavity beam waists may be created where non-linear crystals and modulators may be conveniently placed [19,20].

Schemes such as injection seeded, injection locked and master-oscillator power amplifiers allow for building high power single-frequency lasers and, of course, this incurs in added complexity and costs. Nevertheless, literature presents several lasers that have high power, stable single-frequency output in a single resonator. Guo et al. [21] demonstrated 50.3 W using a single Nd:YVO_4 crystal longitudinally pumped by 888 nm fiber-coupled diode and, using two Nd:YVO_4 crystals, the same group demonstrated in 2018 a continuous output of 101 W [22]. Together with many improvements, the key to obtain a stable low noise single-frequency was to utilize nonlinear losses to reduce relative intensity noise by inserting a nonlinear crystal in the resonator [23] allowing for suppression of adjacent longitudinal modes and thus obtaining a stable single frequency output. This is the highest reported single frequency output from a single resonator for solid-state laser, to our knowledge.

Regarding Nd:YAG lasers, the highest reported single-frequency output power, to our knowledge, was obtained by Xie et al. [24]. They achieved 31.9 W by utilizing proprietary laser modules with side pumping from diode bars employing birefringence compensation by inserting a waveplate between two identical laser modules. Q-switched operation was reported by Li et al. [25] who reported a ring oscillator with an average output power of 35 W. Other Nd:YAG single frequency ring lasers with higher output power do not consist of a single oscillator to our knowledge.

In this work we are interested in obtaining a single-frequency laser, utilizing Nd:YAG standard of the shelf laser modules. For this purpose, a DSR single-frequency ring oscillator was built using two commercial DPSSL modules, containing side-pumped Nd:YAG rods, with birefringence compensation by means of a half wave plate (HWP) between the rods. The maximum continuous, single-frequency, polarized output power obtained was 55.6 W, which is, to our knowledge, the highest single-frequency continuous output power for a Nd:YAG laser in a single resonator. A

Optics EXPRESS

lithium triborate (LBO) crystal was inserted in the resonator to suppress adjacent modes and allow single frequency output. Cavity analysis and experiments showed that the resonator allowed for easy and continuous tuning of the stability range by adjusting only the distances between the optical components, without the need for specific radii of the cavity mirrors. Moreover, these results, obtained with standard side pumped modules, open the path to a simple and economic solution for a high-power, single-frequency laser source.

2. Design considerations for the bow-tie ring resonator

2.1. *Modeling of a resonator containing a pair of curved mirrors and a single focusing rod*

For the design of the symmetrical ring resonator (Fig. 1), the use of two plane mirrors and one pair of curved mirrors was considered. Under these conditions, the beam waist in the resonator is maximum inside the focusing rods and a beam waist is generated at the opposite side for the case of negative radius of curvature mirrors. When considering positive curvature mirrors, the resonator shows two further beam waists next to the focusing rods and maximum beam radius on the curved mirrors. Astigmatism was kept low by using 5 degrees of incidence angle at the mirrors.

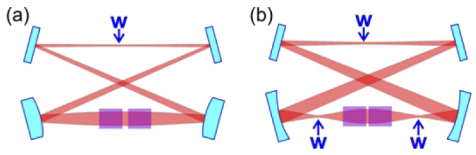

Fig. 1. Scheme of the resonators considered for design with indication of the waist position. (a) With negative curvature mirrors; (b) with positive curvature mirrors.

For better understanding of the dynamic behavior of the resonator, we first consider the case of a resonator with a single rod. Astigmatism is not considered because resonator incidence angle is lower than 5 degrees. Since the resonator is symmetrical, there is only one pair of symmetric mirrors and, therefore, two distances fully define the resonator: distance *a,* which is the distance between the curved mirrors and the rod's principal planes, and distance *b,* the complementary beam travel distance between both plane mirrors. The rods are considered as a lens-like medium with quadratic refractive index variation that can be treated as thin lenses, as discussed in [13], with the beam propagation outside the rod being the same and the beam waist at the thin lens being approximately the beam waist at the rod's principal planes, which are located at a distance *l/(2n)* of the rod's end, where l is the rod's length and n is its refractive index. Real resonator length L is $L = 2a + b + l(1 - 1/n)$. Figure 2 shows the resonator parameters considered in resonator modeling. It should be pointed out that depending on distances a and b it could be necessary to add more pairs of flat folding mirrors, however, as this does not alter any characteristics of the beam propagation they need not to be considered in the modeling. Notice that even though a bow-tie resonator is shown in the picture, it is only to illustrate a possible configuration. The results apply to any resonator where distances a and b are present and astigmatism is negligible.

The resonator was analyzed according the formalism used by Silvestri et al. [18]. The scheme of resonator elements is displayed in Fig. 3. The standard ABCD round-trip matrix for the resonator without the focusing rod is:

$$\begin{pmatrix} A & B \\ C & D \end{pmatrix} = \begin{pmatrix} 1 & a \\ 0 & 1 \end{pmatrix} \cdot \begin{pmatrix} 1 & b \\ -2/R & 1 - 2b/R \end{pmatrix} \cdot \begin{pmatrix} 1 & a \\ -2/R & 1 - 2a/R \end{pmatrix} \tag{1}$$

Optics EXPRESS

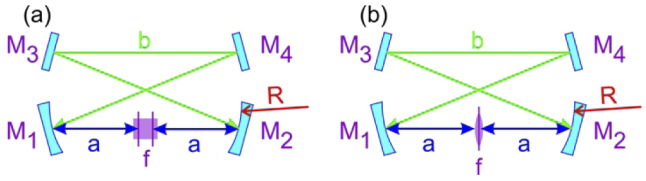

Fig. 2. Resonator parameters utilized for the modeling. a is the distance between the curved mirrors and the rod's principal plane, b is the resonator complementary distance. M_1 and M_2 are mirrors with radius of curvature R while M_3 and M_4 are plane mirrors. (a) Resonator considered; (b) simplification assuming the focusing rod as a thin lens.

And the ABCD matrix elements are:

$$\begin{aligned} A &= 1 - \tfrac{2b}{R} - \tfrac{4a}{R} + \tfrac{4ab}{R^2} \\ B &= a + b - \tfrac{2ab}{R} - \tfrac{2a^2}{R} + a\left(1 - \tfrac{2b}{R}\right)\left(1 - \tfrac{2a}{R}\right) \\ C &= \tfrac{4b}{R^2} - \tfrac{4}{R} \\ D &= \left(1 - \tfrac{2b}{R}\right)\left(1 - \tfrac{2a}{R}\right) - \tfrac{2a}{R} \end{aligned} \tag{2}$$

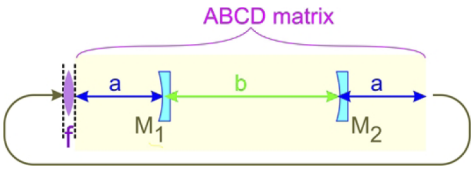

Fig. 3. Scheme of simplified resonator considered for modeling. f represents focusing rod's equivalent thin lens. M_1, M_2, curved mirrors with radius of curvature R.

The limits of the stability interval are given by [18]:

$$\frac{A + D - 2}{B} < \frac{1}{f} < \frac{A + D + 2}{B} \tag{3}$$

The lower limit of (A + D-2) / B gives the lowest dioptric power, that is, the longest length of the thermal lens, equivalent to f_{max}. Similarly, the higher limit gives the shortest thermal lens f_{min}. Substituting the terms of the ABCD matrix in Eq. (3) and simplifying the expressions, we obtain:

$$f_{\max} = \frac{2a - R}{4} \tag{4}$$

$$f_{\min} = \frac{2ab - 2aR - bR}{4(b - R)} \tag{5}$$

By subtracting Eq. (5) from Eq. (4) we obtain:

$$\Delta_f = \frac{R^2}{4(b - R)} \tag{6}$$

By analyzing the expressions above it can be noticed that this resonator has many remarkable characteristics. The existence of these simple analytical expressions allows for quick designing a dynamically stable ring resonator based on the stability interval limits. For a given radius of curvature of the mirrors, the maximum focusing distance f_{max} and the width of the stability

Optics EXPRESS

interval Δ_f are independent, the first being dependent only on distance a and the second dependent only on distance b. This feature is not observed in linear resonators with joint stability zones [26]. The parameters of the stability interval thus is defined by these two parameters f_{max} and Δ_f that depend on distances a and b. The stationary waist w_{30} depends on the stability interval width (in terms of 1/f) [18].

Figure 4(a) shows the beam waist at the rod in the stability interval showing its limits defined in terms of distances a and b. As can be seen, it is not necessary to choose a particular radius of curvature for meeting a desired stability interval set of parameters. Once the radius of curvature of the mirrors is chosen, the resonator stability interval can be continuously adjusted by changing distances a and b, which can be used to fine tune the physical resonator until the best operating point is obtained. Figure 4(b) illustrates the effects of the changes in distances a and b on the stability interval. Increasing the distance a shifts the stability interval to longer focusing lengths while keeping the same width of the stability range Δf. Increasing distance b decreases the stability interval Δf while maintaining the same maximum focusing length f_{max}. It should be pointed out that similar figures are obtained when considering other convex or concave mirrors for different f-values (see Eq. (4) and Eq. (6)). By analyzing Eq. (4) and Eq. (6) we note that, for obtaining positive distances a and b, the mirrors' curvature radius R must either be positive or lie in the interval $-4f_{max}<R<-4\Delta f$. The expressions can be readily utilized for astigmatic resonators simply by replacing the radius of curvature R by the effective radius of curvature $R\cos\theta$ at the tangential and $R/\cos\theta$ at the sagittal planes, with θ being the incidence angle at the curved mirrors. Non normal incidence at the flat mirrors does not modify the expressions. Next, these results are applied to resonators containing two rods close to each other.

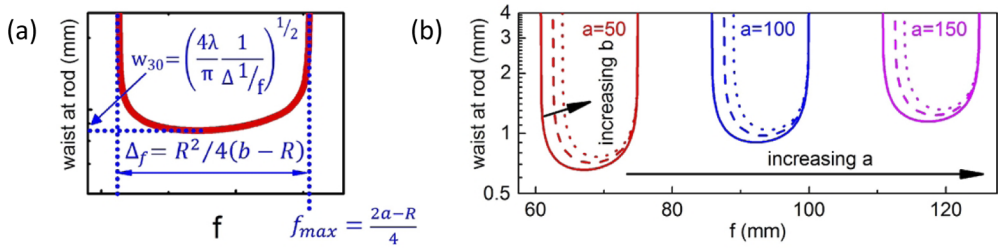

Fig. 4. (a) Laser waist at rod, indicating the parameters of the stability interval in terms of the distances a and b and the radius of curvature of the mirrors. (b) Calculated beam waist showing the tunability of the laser stability interval as a function of the rod's average thermally induced lens. Continuous line: b = 500 mm; dashed line: b = 600 mm; dotted line: b = 700 mm. Mirror radius is R = –200 mm.

2.2. *Modeling of a resonator containing a pair of curved mirrors and two focusing rods*

In order to extend the results to the case of a resonator containing two rods, the focusing length of the thermal lens of the focusing rod f in Eq. (4) and Eq. (6) was replaced by the equivalent focusing length of the set of two lenses f_{eq} and, furthermore, the distance a had to be replaced by the distance a' to take in account the new position of the principal plane of the set of two rods. Figure 5 shows the scheme of the resonator showing the parameters utilized in the modeling.

Equivalent focusing length of a set of two lenses for $f_1=f_2=f$ is given by [27]:

$$f_{eq} = \frac{f^2}{2f-d} \tag{7}$$

The distance h from the set's principal plane to the end of the set is given, for $f_1=f_2=f$, by [27]:

$$h = \frac{fd}{2f-d} \tag{8}$$

Optics EXPRESS

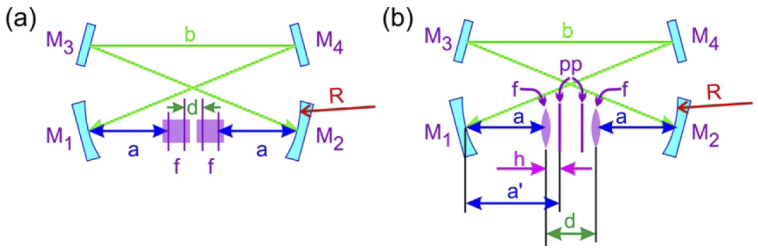

Fig. 5. Parameters for the resonator containing two focusing rods f whose principal planes are separated by a distance d. The distance between the curved mirrors to the rod's principal plane is *a* and b is the resonator complementary distance. M_1 and M_2 are mirrors with radius of curvature R while M_3 and M_4 are plane mirrors. pp are principal planes of the set of two lenses. *a'* is the distance between curved mirrors and the principal plane of the set of two rods. (a) Resonator considered; (b) simplification assuming the focusing rods as thin lenses.

Replacing the f_{max} value by $f_{\max\ eq} = f_{\max}{}^2/2f_{\max} - d$ (according to Eq. (8)) and distance a by $a'=a+h$ in Eq. (4) we obtain:

$$f_{\max} = a - \frac{R}{2} \tag{9}$$

whose value is exactly the double of Eq. (4). Writing $\Delta_{f\ eq} = f_{\max\ eq} - f_{\min\ eq}$ and utilizing Eq. (7) the following expression is obtained:

$$\Delta_{f\ eq} = \frac{(f_{\max} - f_{\min})(2f_{\max}f_{\min} - df_{\max} - df_{\min})}{2(2f_{\max}f_{\min} - df_{\max} - df_{\min} + d^2/2)} \tag{10}$$

If the rods are positioned close to each other, $d<<f_{max}$ and $d<<f_{min}$ and, therefore, $d^2/2$ in the denominator can be omitted. By doing this approximation and replacing the result in Eq. (6) we obtain:

$$\Delta f = \frac{R^2}{2(b-R)} \tag{11}$$

To check the approximation, we compared the value of Δ_f calculated using Eq. (11) with results obtained from simulations using the software LASCAD. These simulations took in account d=72 mm, which was the spacing between the principal planes of our laser modules and the distances *a* ranging from 50 mm to 500 mm, b ranging from 100 to 6854.8 mm and *R* values ranging from –300 mm to 500 mm. The results presented good compliance with the simulations with a maximum error of less than 1%. Results of the comparison are shown in Fig. 6. Similarly to the case of a single rod, in order to obtain positive distances *a* and *b*, curvature radius must either be positive or, in the case of negative radius, lie in the interval $-2f_{max}<R<-2\Delta$f, as can be concluded by analyzing Eq. (9) and Eq. (11). In short, both expressions for f_{max} and Δf are the same for two rods positioned close to each other, as well as for a single rod observing a factor of 2, as can be seen by comparing Eq. (4) with Eq. (9) and Eq. (6) with Eq. (11). Thus, the resonators, either with a single rod or with two rods positioned close to each other, have the same behavior regarding the tunability of the stability interval.

2.3. Design of the resonator

The laser modules had Ø3 mm x 78 mm Nd:YAG rods each, doped with 0.6 at.% neodymium and pumping was performed by 12 diode bars emitting at 808 nm disposed in groups of four in a three-fold geometry. Each module had a maximum pump power of 225 W. The modules minimum average focal length was 21.5 cm. The resonator was designed to have its stability limit at the lowest focusing distance (highest dioptric power) of f = 21 cm. The rod's thermal

Optics EXPRESS

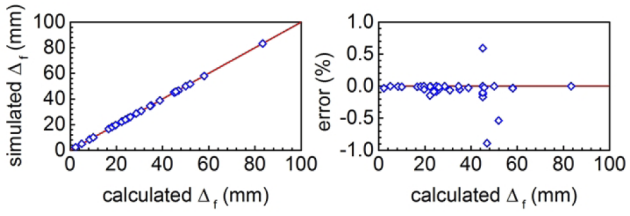

Fig. 6. Comparison between Δ_f values calculated with Eq. (11) and obtained in simulations.

lens was measured by passing a collimated He-Ne laser beam through the pumped rods, using a slit and a polarizer before the rods, allowing radial and tangential components to be measured separately as described in [8]. Beam waist was assigned to be 762 µm; the same value achieved good results in a previous work that used the same modules in a linear resonator [17]. The mirror radius of curvature used in our set-up was 500 mm and the corresponding distances *a* and *b* were 528 mm and 2284 mm, respectively. Figure 7(a) shows the resulting beam waist in the stability interval of the resonator. Incidence angle on the mirrors was 5° allowing for minimal astigmatism. Figure 7(b) shows the beam waist at maximum pump power along the resonator path.

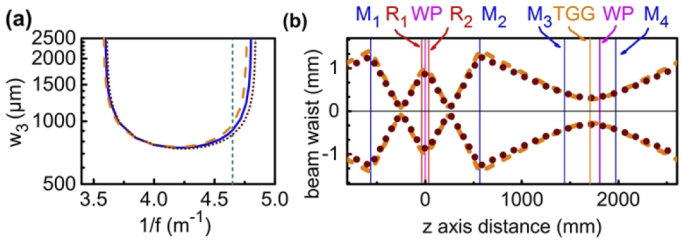

Fig. 7. (a) Simulated TEM_{00} beam waist at rod as a function of dioptric power. The continuous line represents the normal incidence while dashed and dotted lines represent x and y planes, respectively for 5° incidence angle at the mirrors. (b) Simulated TEM_{00} waist along the resonator at maximum pump power. Dashed: x-plane; dotted line: y-plane. Position of the elements is indicated at the top of the graph. M_1, M_2: curved mirrors; M_3: plane mirror; M_4: output coupler; R_1 and R_2: laser rods; WP: half wave plate; TGG: Faraday rotator. The vertical line in (a) represent the focal length of the thermal lens at maximum pump power.

2.4. Design considerations for birefringence compensation

The horizontally polarized laser was composed of two identical laser modules with a HWP in between them. Rays that propagate along the horizontal or vertical planes of the rod axis become r-polarized or t-polarized, respectively. These rays do not suffer depolarization and are not affected by the HWP. A ray that travels in between both planes is decomposed in radial and tangential polarized rays by the thermally induced birefringence of the first rod. For birefringence compensation to occur, both polarized rays must pass through the system suffering the same phase delay and average thermally induced lens. The HWP between both rods guarantees that the radially polarized beam exiting the first rod becomes tangentially polarized in the second rod, and vice versa. A t-polarized ray at the entrance of the second rod will experience birefringence compensation if the phase delay and thermally induced lens in the second rod is the same as for the t-polarization in the first rod (and vice versa). For this scheme to work properly, the distance from the rod axis must be the same in both rods because of the radial dependence of the thermal effects.

Optics EXPRESS

The use of a single HWP between both rods requires a total of two roundtrips before a ray acquires again the same polarization, as shown in Fig. 8(c). This implies in the rays passing twice through a rod with the same polarization, thereby suffering the same thermal lens and experiencing quite different dioptric powers depending on polarization. The use of a second HWP, as shown in Fig. 8(d), could improve performance because beam polarization status would be alternated every time the beam passes through a rod, which should result in a ray experiencing a more constant dioptric power and, therefore, with more constant beam distances from the resonator axis. Considering that the resonator needs one more HWP for the non-reciprocal device (Faraday rotator), the use of three HWP in the resonator does complicate laser optimization once the rotation of any of the HWP changes the polarization status in the whole system.

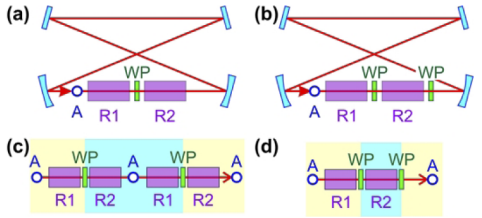

Fig. 8. Scheme illustrating birefringence compensation utilizing one (a) or two (b) half wave plates (WP). Evolution of the polarization across the resonator axis during a complete cycle starting and finishing in point A is indicated for the resonators with one (c) and two half wave plates (d). Different background colors indicate different polarization states (radial or tangential). For one WP, a complete cycle takes 2 round trips in the resonator and rays always pass through two rods with the same polarization before changing its polarization state while for 2 WPs, complete cycle takes one resonator round trip and radial and tangential thermal lenses alternate each time it passes through a rod.

To check if there exists a large change in beam radius when using only one HWP, rather than using two HWPs, the resonator of our set-up was simulated (LASCAD GmbH). The rod thermal lens at maximum pump power was approximated by a set of 7 lenses with $f_\phi = 1597$ mm and $f_r = 1320$ mm separated by 11.14 mm from each other, corresponding to a total rod length of 78 mm, and an average focal length of 21.5 cm (f_ϕ=23.65 cm and fr = 19.71 cm), which corresponds to earlier experimentally measured rod focal lengths at maximum pump power for this type of DPSSL modules [17]. The ratio between radial and tangential lens was $f_\phi/f_r = 1.2$, as previously established [4].

Figure 9(a) shows the behavior of the beam waist that is either radially or tangentially polarized as it passes through the first and second rod. A ray that propagates radially polarized in the first rod has a larger radius than a tangentially polarized ray in the same rod. When the first ray enters the second rod with exchanged polarization state, it becomes tangentially polarized and has smaller radii than a radially polarized ray as seen in Fig. 9(a). The behavior is symmetric, i.e. the radius as a function of distance of a tangentially polarized ray travelling through the first rod is the same as for a tangentially polarized ray travelling through the second rod. Differences between the radii for one and two round trips are minimal and shown in Fig. 9(b) where the ratios of radial and tangential radii inside the rod are plotted. A slightly better result is obtained by using only one HWP instead of two. It is important to point out that the plotted waist values in this figure are larger than the 762 µm value of the stationary waist described above, as 762 µm is the waist size in the middle of the stability interval and not at maximum pump power. The simulation shows the waist at maximum pump power represented as the vertical line in Fig. 7(a).

Optics EXPRESS

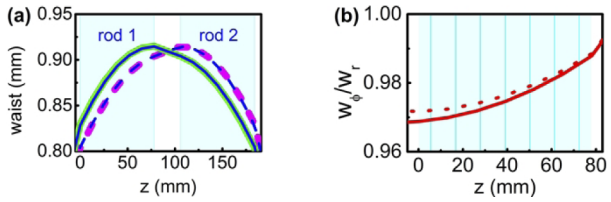

Fig. 9. (a) Beam radius as it propagates along the resonator axis z through the 2 rods. The continuous lines represent a ray that passes with radial polarization in the first rod and tangential polarization in the second rod while the dashed lines represent a ray that propagates with tangential polarization in the first rod and radial polarization in the second rod. Thick lines represent values obtained for one round trip and thin lines represent values obtained for two round trips. (b) Represents the ratio between radial and tangential radii along the first rod for one round trip (continuous line) and two round trips (dotted line). Vertical lines indicate the position of the seven lenses considered in the simulations.

3. Results

Figure 10 shows the combined output power of the two output beams obtained for different output coupler reflectivities without the Faraday rotator inside the resonator (Fig. 10(a)) and for the unidirectional resonator with Faraday rotator (Fig. 10(b)). The output coupler with 35% transmission resulted in the highest output power and was used in the following experiments for the bidirectional resonator while the 25% transmission mirror provided highest output for the unidirectional resonator, because losses were added by introducing the non-reciprocal device.

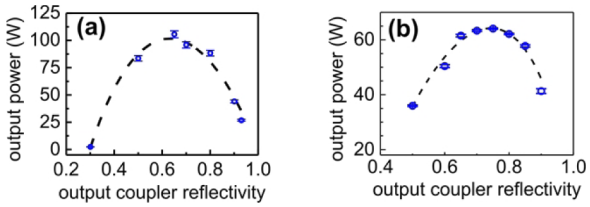

Fig. 10. Continuous laser output power as a function of output coupler transmission. (a) Total output power when resonator was running bidirectionally. (b) Output power when resonator was running unidirectionally.

In the absence of a polarizing element (Faraday rotator), the laser showed 76% of polarization in the horizontal direction with 106.3 W of maximum bidirectional output power. Insertion of the HWP for birefringence compensation improved the beam quality from M^2_x=2.42 and M^2_y=4.02 to M^2_x=1.71 and M^2_y=1.56 with a slightly smaller output power of 96 W. Figure 11(b) and Fig. 11(c) shows the beam profiles and the waists obtained with a scanning slit device (Beamscope P8, Dataray) using second moment integration. For comparison with the polarized and unidirectional beam operation, a quartz Brewster plate was inserted in the bidirectional resonator between mirrors M_3 and M_4 resulting in a further power decrease (91 W) but higher degree of polarization of 86.6%. Output powers at maximum pump power and degree of polarization are plotted in Fig. 11(a).

Next, the Faraday rotator was inserted in the resonator to obtain unidirectional operation. The non-reciprocal device consisted of a 6 mm long terbium gallium garnet (TGG) crystal cut at Brewster's angle inside strong magnets and a HWP. Measured polarization rotation by the TGG was 6 degrees. Unidirectional output power dropped to 62 W. Part of this drop can be attributed to the additional polarizing function of the Brewster cut TGG. The longitudinal mode spectrum, obtained with a Fabry-Perot scanning interferometer (HiFase, Burleigh) with FSR of 74 GHz, is

Optics EXPRESS

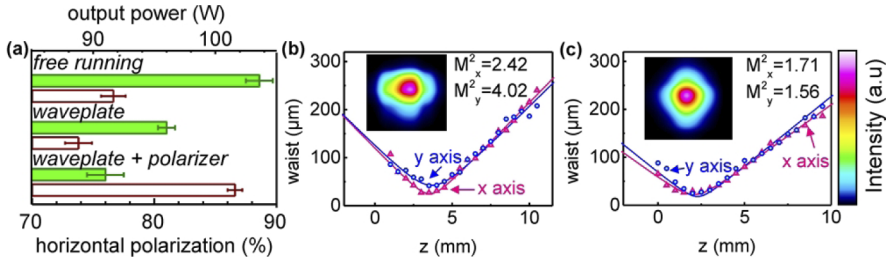

Fig. 11. (a) Bidirectional laser output powers (filled bars) and percent of polarized output (white bars) at maximum pump power obtained without the etalon. (b) Second moment waist radius along z axis during bidirectional operation without half wave plate and (c) with half wave plate for birefringence compensation. Insets show far field intensity profiles obtained with a scanning slit device.

shown in Fig. 12(a) (inset). It can be noted that besides the central peak there are two additional peaks separated by 1027 MHz that correspond to approximately the length of the laser rods (Fig. 12(a), bottom waveform). The waveform was not stable and intermittent small peaks with a spacing of about 80 MHz that are compatible with the resonator longitudinal mode separation can also be seen (top waveform).

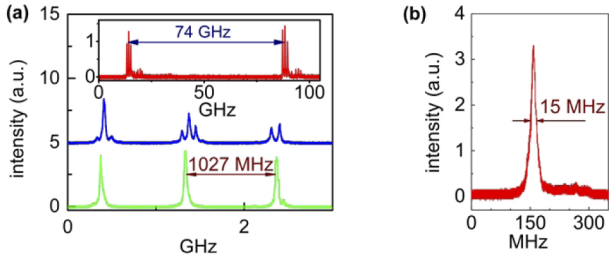

Fig. 12. (a) Two instances of longitudinal mode structure without intracavity etalon measured with the scanning Fabry-Perot etalon during unidirectional laser operation. Inset shows a full free spectral range of the scanning etalon. (b) Laser spectrum showing the single-frequency output obtained with the use of the intracavity etalon.

Using a 10 mm long uncoated fused silica etalon with a 15.66 GHz free spectral range (FSR), it was possible to obtain single frequency operation with a 15 MHz line width. Setup is shown in Fig. 13. The spectrum obtained with a 16.3 GHz scanning etalon is shown in Fig. 12(b). Maximum output power was 51.6 ± 1.5 W. Beam quality was M^2_x=1.26 and M^2_y=1.49 indicating near-diffraction limited beam quality (Fig. 14(b)). Differences in x and y directions are due to differences in the polarization components of the rod's thermal lens due to inhomogeneity in the pump, which leads to different focusing lengths in x and y directions when polarized [26,28]. Input-output power curves for the single-frequency laser compared to the resonator without the etalon and the bidirectional resonator are shown in Fig. 14(a).

During unidirectional operation, some flickering on the second output of the laser was observed and, during those moments, the main output ceased, i.e., the laser ran briefly unidirectional in the other direction each time output 2 flickered. This could be a result from the isolator losses not being high enough to assure perfect unidirectional operation. In order to prevent the laser to run in the reverse direction, a feedback mirror was positioned at the secondary output of the laser, in the position corresponding to the image of the waist at the TGG crystal, to mitigate the occurrence of a counter propagating wave and improve frequency stability. Additionally, a

Optics EXPRESS

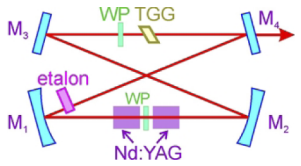

Fig. 13. Resonator scheme for the unidirectional operation with the etalon.

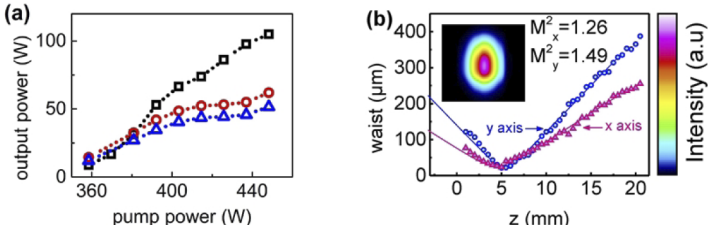

Fig. 14. (a) Laser output power curve for operation in bidirectional (squares) mode, unidirectional (circles) mode and with the intracavity etalon (triangles). (b) Second moment waist radius along z axis with M^2 fit and far field transversal intensity profile of the unidirectional laser (inset) obtained with a scanning slit device.

$4 \times 4 \times 20$ mm^3 type I, non-critical phase-matched lithium triborate (LBO) crystal was inserted in the resonator in the waist between the rod and the curved mirror (Fig. 15) in order to enhance single longitudinal mode as a result of different nonlinear losses between adjacent laser modes [22,29,30]. Also, a dichroic mirror was inserted in the resonator to extract the 532 nm light. The effective output power measured from mirror M_4 was 34.8 ± 0.5 W due to the fact that the available LBO crystal was not optimized regarding its coatings: a 6% reflection loss at 1064 nm at each face was measured. Intracavity power reflected from the LBO crystal faces was measured and counted as laser output power and the output coupler was replaced by a mirror with 20% transmission so that total output power extracted was still close to the value of the optimized output coupler. The scheme of the setup is displayed in Fig. 15. The laser output power with the feedback mirror and with the phase matched LBO was 55.6 ± 0.9 W while 532 nm output power was 840 ± 20 mW.

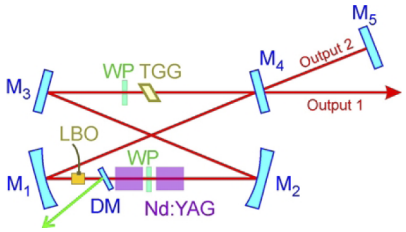

Fig. 15. Scheme of the resonator with LBO and feedback mirror. M_1, M_2 are 500 mm radius mirrors; M_3 flat mirror; M_4 flat output coupler; M_5 flat HR feedback mirror; WP half wave plate; DM dichroic mirror.

To characterize single-frequency stability, the peak of the scanning Fabry-Perot interferometer signal was recorded for each oscilloscope scan. Interval between data was limited by the oscilloscope acquisition time and 1000 scans were recorded in about 70 s. The results obtained with or without the feedback mirror and for LBO with or without phase matching (PM) are shown in Fig. 16. The left part of Fig. 16 shows the recorded values while the right side shows a

Optics EXPRESS

histogram for each curve. The scale of the histogram is logarithmic to help observing frequencies of only a few counts. It is possible to note large mode hops that could be only suppressed when both, feedback mirror and LBO phase matching, were present. In this condition, the laser hopped across about ±10 resonator modes as can be seen in the inset of Fig. 16.

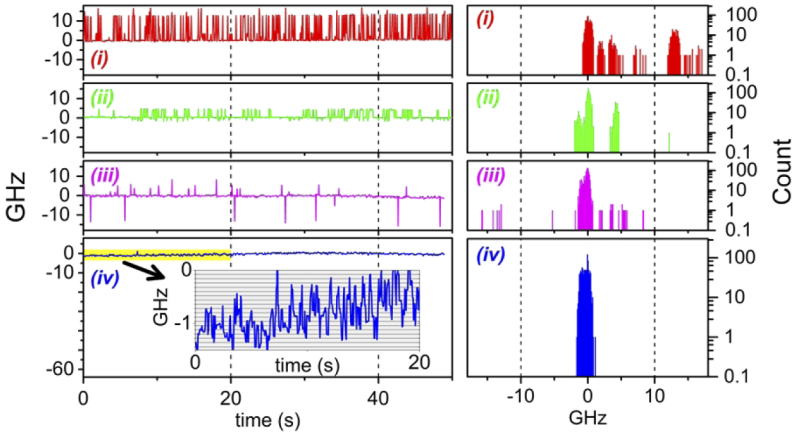

Fig. 16. Frequency (left) and histogram of data (right) measured during unidirectional operation (i) without PM and without feedback mirror, (ii) without PM with feedback mirror; (iii) with PM and without feedback mirror; (iv) with PM and feedback mirror. Graphics at right have the same horizontal scale for comparison purposes. Graphics at left have the same horizontal scale except for the inset that is expanded. Inset shows first 20 s of (iv) with enlarged scale with horizontal lines representing spacing between resonator longitudinal modes.

A Gaussian was adjusted to the histogram data to evaluate the frequency stability and its FWHM was 1.5 GHz (Fig. 17(a)). A line width of 29 MHz was measured from the scanning etalon signal (Fig. 17(b)). This line width value is greater than the value measured with the 10 mm etalon in the resonator (shown in Fig. 12(b)), however the 29 MHz width represents a typical waveform from a noticeably more stable frequency output while the 15 MHz line width measured at Fig. 12(b) is the best performance measurement in a much less stable waveform. The presence of a single frequency can be seen in Fig. 17(c) where about ten scanning signals for each condition were overlapped and the curves were translated to keep central frequency in the center of the horizontal axis. When the laser ran without the LBO PM (curve i) about 10 longitudinal modes were present (not simultaneously) together with the central frequency. When the feedback mirror is added, less modes are present (curve ii) and when the LBO enters in PM, additional frequencies are suppressed (curve iii). Laser beam quality was measured to be $M^2_x = 1.11$ and $M^2_y = 1.25$ (Fig. 18) and of 97.89(12)% horizontal polarization. This high degree of polarization is due to the stronger polarization introduced by the TGG when compared to the quartz plate.

3.1. Comparison with standing wave resonator

Recently a polarized Nd:YAG standing wave resonator using the same two diode pump modules was built [17]. Although the standing wave resonator was much shorter, (53.6 cm overall length), a TEM_{00} polarized output of 76.3 W was obtained, which is 23% higher than the present ring resonator. The linear cavity was the result of a process of successive developments that allowed for such a high-power, polarized, high beam quality to be obtained from standard commercial modules [16,26,31,32]. The current work is the first using these modules in a ring cavity and improvements are still expected, particularly owing to the favorable design characteristics of the

Optics EXPRESS

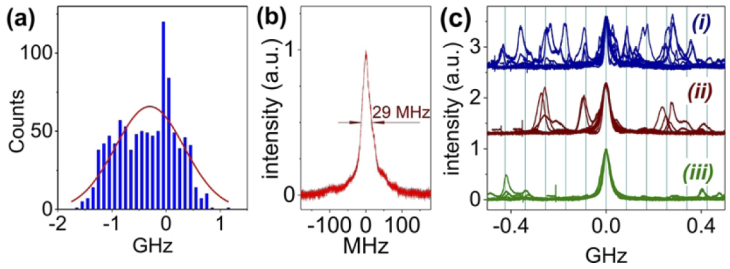

Fig. 17. (a) Histogram of time frequency stability data measured during unidirectional operation with PM and feedback mirror with a Gaussian fit. (b) Linewidth measurement with PM and feedback mirror. (c) Overlapped signals from scanning etalon translated to keep central frequency in the middle of the horizontal axis for the resonator without PM and feedback mirror (i), adding feedback mirror (b), and with PM and feedback mirror together (iii). Vertical lines in (c) represent spacing between longitudinal modes.

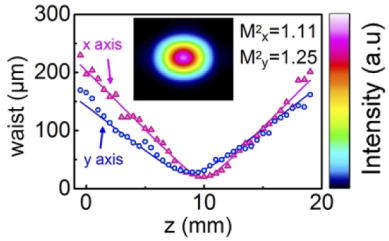

Fig. 18. Second moment waist radius along z axis with M^2 fit and far field transversal intensity profile (inset) of the laser with LBO PM and feedback mirror, obtained with a scanning slit device.

resonator regarding the tuning of the stability range independently of distances *a* and *b* and the possibility of using astigmatism of curved mirrors to compensate the bi-focusing.

Optics EXPRESS

4. Conclusions

The results presented here, using Nd:YAG as the active media and employing mode filling for obtaining a dynamically stable resonator, demonstrate a cost efficient solution incorporating standard, side-pumped diode modules. We analyzed the case of a symmetric dynamically stable ring resonator with a pair of curved mirrors and showed that ring resonators are very favorable for mode filling and, thus, near-diffraction limited operation. Stationary beam waist size, beginning and width of stability interval are easily, independently, continuously and precisely determined just by changing distances between resonator components, thus allowing for tuning stability limits under lasing condition until reaching the optimum results. Additionally, the detrimental effects of thermally induced birefringence can be effectively and efficiently eliminated. Further improvements could be obtained by the inclusion of an active stabilization device, such as an active mirror, for maintaining the same single-frequency wavelength.

The single-frequency laser output power reported here is, to our knowledge, the highest reported so far in the literature obtained for Nd:YAG without the use of amplifiers or seeding sources. A maximum, 98% polarized, single-frequency output power of 55.6 W with M^2 of 1.11×1.25 (h x v) was obtained. Compared to other gain materials used in non-amplified, single-frequency ring resonators, there has been only a single, very recent work by Guo et al. [21] with better results, that employed two naturally birefringent Nd:YVO crystals, longitudinally pumped by fiber-coupled diodes in a much more complex set-up to achieve 100 W of output power.

Funding. Coordenação de Aperfeiçoamento de Pessoal de Nível Superior; Fundação de Amparo à Pesquisa do Estado de São Paulo (2017/05854-9, 2017/10765 5).

Disclosures. The authors declare no conflicts of interest.

Data availability. Data underlying the results presented in this paper are not publicly available at this time but may be obtained from the authors upon reasonable request.

References

1. O. Gail and S. Anderson, "LASER MARKETPLACE 2009: Photonics enters a period of high anxiety," https://www.laserfocusworld.com/test-measurement/research/article/16566015/laser-marketplace-2009-photonics-enters-a-period-of-high-anxiety.
2. G. Overton, "Laser revenues on track to exceed $9 billion by 2015, says Strategies Unlimited," (n.d.).
3. W. Koechner, "Properties of Solid-State Laser Materials," in *Solid-State Laser Engineering* 16th ed. (Springer, 2006), pp. 38–101.
4. W. Koechner, "Thermo-Optic Effects," in *Solid-State Laser Engineering* 16th ed. (Springer, 2006), pp. 423–487.
5. J. D. Foster and L. M. Osterink, "Thermal effects in a Nd:YAG laser," J. Appl. Phys. **41**(9), 3656–3663 (1970).
6. W. C. Scott and M. De Wit, "Birefringence compensation and tem00 mode enhancement in a Nd: Yag laser," Appl. Phys. Lett. **18**(1), 3–4 (1971).
7. W. a Clarkson, N. S. Felgate, and D. C. Hanna, "Simple method for reducing the depolarization loss resulting from thermally induced birefringence in solid-state lasers," Opt. Lett. **24**(12), 820–822 (1999).
8. N. U. Wetter, E. P. Maldonado, and N. D. Vieira, "Enhanced efficiency of a continuous-wave mode-locked Nd:YAG laser by compensation of the thermally induced, polarization-dependent bifocal lens," Appl. Opt. **32**(27), 5280 (1993).
9. Q. Lu, N. Kugler, H. Weber, S. Dong, N. Muller, and U. Wittrock, "A novel approach for compensation of birefringence in cylindrical Nd: YAG rods," Opt. Quantum Electron. **28**(1), 57–69 (1996).
10. M. Ostermeyer, G. Klemz, P. Kubina, and R. Menzel, "Quasi-continuous-wave birefringence-compensated single- and double-rod Nd:YAG lasers," Appl. Opt. **41**(36), 7573–7582 (2002).
11. M. Frede, R. Wilhelm, D. Kracht, and C. Fallnich, "Nd:YAG ring laser with 213 W linearly polarized fundamental mode output power," Opt. Express **13**(19), 7516 (2005).
12. Y. Wang, H. Kan, T. Ogawa, and S. Wada, "Optimization of two-lens coupling structure for a tandem-set solid-state laser system," J. Opt. **12**(8), 085702 (2010).
13. V. Magni, "Resonators for solid-state lasers with large-volume fundamental mode and high alignment stability," Appl. Opt. **25**(1), 107 (1986).
14. M. P. Murdough and C. a Denman, "Mode-volume and pump-power limitations in injection-locked TEM_00 Nd:YAG rod lasers," Appl. Opt. **35**(30), 5925 (1996).
15. G. Cerullo, S. de Silvestri, V. Magni, and O. Svelto, "Output power limitations in CW single transverse mode Nd: YAG lasers with a rod of large cross-section," Opt. Quantum Electron. **25**(8), 489–500 (1993).

Optics EXPRESS

16. R. S. D. S. Pinto and N. U. Wetter, "Highly efficient, dynamically stable Nd: YAG single-rod resonators with 60% TEM 00 extraction efficiency and high misalignment stability," Laser Phys. **24**(8), 085801 (2014).
17. A. Bereczki and N. U. Wetter, "100W continuous linearly polarized, high beam quality output from standard side-pumped Nd:YAG laser modules," Opt. Laser Technol. **96**, 271–275 (2017).
18. S. De Silvestri, P. Laporta, and V. Magni, "Rod thermal lensing effects in solid-state laser ring resonators," Opt. Commun. **65**(5), 373–376 (1988).
19. T. A. King, "Ring Laser Resonators," in *The Physics and Technology of Laser Resonators*, D. R. Hall and P. E. Jackson, eds., 1st ed. (Adam Hilger, 1989), pp. 62–79.
20. A. E. Siegman, "Unidirectiona ring-laser oscillators," in *Lasers*, University Science Books, ed., 1st ed. (1986).
21. Y. Guo, H. Lu, M. Xu, J. Su, and K. Peng, "Investigation about the influence of longitudinal-mode structure of the laser on the relative intensity noise properties," Opt. Express **26**(16), 21108 (2018).
22. Y. Guo, M. Xu, W. Peng, J. Su, H. Lu, and K. Peng, "Realization of a 101 W single-frequency continuous wave all-solid-state 1064 nm laser by means of mode self-reproduction," Opt. Lett. **43**(24), 6017 (2018).
23. H. Lu, Y. Guo, and K. Peng, "Intensity noise manipulation of a single-frequency laser with high output power by intracavity nonlinear loss," Opt. Lett. **40**(22), 5196 (2015).
24. S.-Y. Xie, Y. Bo, J.-L. Xu, Z.-C. Wang, Q.-J. Peng, D.-F. Cui, and Z.-Y. Xu, "A High Power Single Frequency Diode Side-Pumped Nd:YAG Ring Laser," Chinese Phys. Lett. **28**(8), 084207 (2011).
25. Y. Li, W. Tu, B. Wang, N. Zong, F. Yang, F. Zhang, S. Zhang, Z. Wang, Q. Peng, D. Cui, and Z. Xu, "High-Power Narrow-Linewidth Q-Switched TEM 00 Mode 355-nm Laser," IEEE Photonics J. **10**(3), 1–9 (2018).
26. A. Bereczki, M. A. P. Aparício Lopez, and N. U. Wetter, "Dynamically stable Nd:YAG resonators with beam quality beyond the birefringence limit and pumping of a singly resonant optical parametric oscillator," Opt. Lett. **43**(4), 695 (2018).
27. D. Malacara-Hernández and Z. Malacara-Hernández, "Systems of Several Lenses and Thick Lenses," in *Handbook of OPTICAL DESIGN*, 1st ed. (Marcel Dekker, 2004).
28. A. Bereczki and N. U. Wetter, "Dynamically stable lasers from commercial Nd:YAG modules with high beam quality and single-frequency: The correct choice of the fundamental waist size at the rod," in *Laser Resonators, Microresonators, and Beam Control XXII*, A. M. Armani, A. V. Kudryashov, A. H. Paxton, and V. S. Ilchenko, eds. (SPIE, 2020), p. 43.
29. H. Lu, J. Su, Y. Zheng, and K. Peng, "Physical conditions of single-longitudinal-mode operation for high-power all-solid-state lasers," Opt. Lett. **39**(5), 1117 (2014).
30. S. Greenstein and M. Rosenbluh, "The influence of nonlinear spectral bandwidth on single longitudinal mode intra-cavity second harmonic generation," Opt. Commun. **248**(1-3), 241–248 (2005).
31. R. de Souza Pinto and N. U. Wetter, "Highly efficient TEM00 mode operation of a diode-side-pumped Nd:YAG rod Laser," in *Advanced Solid-State Lasers Congress* (OSA, 2013), p. ATu3A.14.
32. R. de Souza Pinto, D. Geskus, and N. U. Wetter, "45W CW TEM00 mode diode-side-pumped Nd:YAG rod laser with linearly polarized beam," in *CLEO: 2014* (OSA, 2014), p. JTh2A.82.